Int J Ind Chem (2015) 6:105–117
DOI 10.1007/s40090-015-0037-9

RESEARCH

Synthesis, characterization and inhibition effect of new antipyrinyl derivatives on mild steel corrosion in acidic solution

Mahmoud N. El-Haddad[1] · **Khaled M. Elattar**[1]

Received: 16 September 2014 / Accepted: 19 March 2015 / Published online: 16 April 2015

Abstract Newly antipyrinyl derivatives **4** and **5** were synthesized from the reaction of enaminonitrile 3 with 1-nitroso-2-naphthol and salicyaldehyde, respectively, and used to protect mild steel dissolution in 1.0 M HCl solutions using weight loss, potentiodynamic polarization, and electrochemical impedance spectroscopy measurements. It was shown that these inhibitors act as good corrosion inhibitors for mild steel protection. The inhibition efficiencies were attributed to the simple blocking effect by adsorption of inhibitor molecules on the mild steel surface. The results showed that inhibitors acts as a mixed-type inhibitor. Relationship between molecular structure and their inhibition efficiency was elucidated by quantum chemical calculations.

Keywords Mild steel · Weight loss · Polarization · EIS · Acid corrosion · DFT calculations

Introduction

Mild steel is widely used in many industrial applications. In most industrial processes, the acidic solutions are commonly used for the pickling, industrial acid cleaning, acid descaling, oil well acidifying, etc. [1–6]. Corrosion prevention systems favor the use of environmental chemicals with low or zero environmental impacts.

The decreasing corrosion rate of metals provides a saving of resources and economical benefits during the industrial applications as well as increasing the lifetime of equipments and also decreasing the dissolution of toxic metals from the components into the environment. The use of organic molecules as corrosion inhibitor is one of the most practical methods for protecting metals against the corrosion and it is becoming increasingly popular. The existing data show that organic inhibitors act by the adsorption and protect the metal by film formation. Organic compounds bearing heteroatoms with high electron density, such as phosphor, sulfur, nitrogen, oxygen or those containing multiple bonds which are considered as adsorption centers, are effective as corrosion inhibitor [7–19].

In this work, we aimed to synthesize and characterize new heterocyclic compounds to investigate their behavior as new inhibitors for the corrosion of mild steel in 1.0 M HCl solution using chemical and electrochemical techniques. In this context, the effects of the structural changes on the ability of these compounds to act as corrosion inhibitors by theoretical calculations were investigated.

Experimental

Materials and chemicals preparation

The mild steel specimens (0.045 % P; 0.3 % Si; 0.3 % Cr; 0.3–0.65 % Mn; 0.14–0.22 % C; 0.05 % S; 0.3 % Ni; 0.3 % Cu and the remainder Fe) were ground with different emery papers (grade 400, 600, 800, 1000 and 1200) in order to abrade the surface of mild steel from impurities and becomes more smoothing for investigation, rinsed with bidistilled water, degreased with acetone before use, dried and kept in a desiccator at room temperature. All chemicals and solvents used in this study were of analytical grade supplied by Aldrich or Merck and used as received.

✉ Mahmoud N. El-Haddad
noaman_eg@yahoo.com

[1] Chemistry Department, Faculty of Science, Mansoura University, P.O. Box: 35516, Mansoura, Egypt

The test solution (1.0 M HCl) was prepared by dilution of analytical grade 37 % HCl with doubly distilled water. Stock solutions (10^3 μM) of inhibitors were prepared by dissolving an accurately weighed quantity of each inhibitor in (100 ml) absolute ethanol, and then the required concentrations (2.0–8.0 μM) were prepared by dilution with doubly distilled water.

Synthesis and characterization of inhibitors

The synthetic strategies adopted to obtain the target compounds are depicted in Figs. 1 and 2. The starting material, 2-[(1,5-dimethyl-3-oxo-2-phenyl-2,3-dihydro-1*H*-pyrazol-4-yl)-hydrazono] malononitrile (**2**) [20], was prepared by diazo-coupling of 4-aminoantipyrine (**1**) with malononitrile in ethanolic sodium acetate solution at 0–5 °C. Compound (**2**) reacted with piperidine in refluxing ethanol to afford the corresponding 1:1 acyclic enaminonitrile adduct 3-amino-2-((1,5-dimethyl-3-oxo-2-phenyl-2,3-dihydro-1H-pyrazol-4-yl)diazenyl)-3-(piperidin-1-yl)acrylonitrile (**3**) [21], respectively. The formation of enaminonitrile (**3**) was illustrated through the initial addition of the secondary amines to cyano function to form the imino form followed by [1, 5] H migration to form the enamine form (Fig. 1).

On the other hand, cyclocondensation of enaminonitrile derivative (**3**) with 1-nitroso-2-naphthol in refluxing ethanol in the presence of a catalytic amount of TEA to yield antipyrinyl derivative 4-((5-Imino-3-(piperidin-1-yl)-5H-naphtho[2,1-b][1, 4, 5]oxadiazocin-4-yl)diazenyl)-1,5-dimethyl-2-phenyl-1H-pyrazol-3(2H)-one (**4**). In a similar manner, enaminonitrile derivative (**3**) underwent cycloaddition with salicyaldehyde in refluxing ethanol in the presence of a catalytic amount of TEA afforded antipyrinyl derivatives 4-((2-Imino-4-(piperidin-1-yl)-2H-benzo[b][1,5]oxazocin-3-yl)diazenyl)-1,5-di-methyl-2-phenyl-1H-pyrazol-3(2H)-one (**5**) (Fig. 2). The structure of (**4**) was confirmed on the basis of elemental analyses and spectral data. The IR spectra (Fig. 3a) showed the presence of (N=N) group at ν 1579 cm^{-1}. The mass spectra showed the molecular ion peak at *m/z* 520 (M^+, 3.7 %). The reaction proceeded initially via condensation of amino group of compound (**3**) with aldehyde group followed by the addition of hydroxyl group in the aldehyde derivatives to cyano function. The formation of derivative (**5**) is indicated by the presence of (C=N) groups in the IR spectra (Fig. 3b) at ν 1593 and 1614 cm^{-1}, respectively, besides no bands of hydroxyl and cyano groups were observed. The mass spectra gave an additional evidence for structure formation in which the molecular ion peak appeared at *m/z* 387 (M^+-piperidyl, 2 %).

All melting points are recorded on Gallenkamp electric melting point apparatus. The FT-IR spectra υ cm^{-1} (KBr) were run on a Nicolet iS10 FT-IR spectrometer (Thermo, USA). The ^{13}C-NMR and ^{1}H-NMR spectra were run on Varian Spectrophotometer at 100 and 400 MHz, respectively, using tetramethylsilane (TMS) as an internal reference and using dimethylsulfoxide (DMSO-d_6) as solvent. The mass spectra (EI) were run at 70 eV with JEOL JMS600 equipment and/or a Varian MAT 311 A Spectrometer. Elemental analyses (C, H and N) were carried out at the Microanalytical Unit of Mansoura University, Egypt. The results were found to be in good agreement with the calculated values.

Weight loss measurements

The mild steel five specimens of (2.0 cm × 2.0 cm × 0.1 cm) dimensions were abraded with different grades of emery papers, washed with distilled water, degreased with

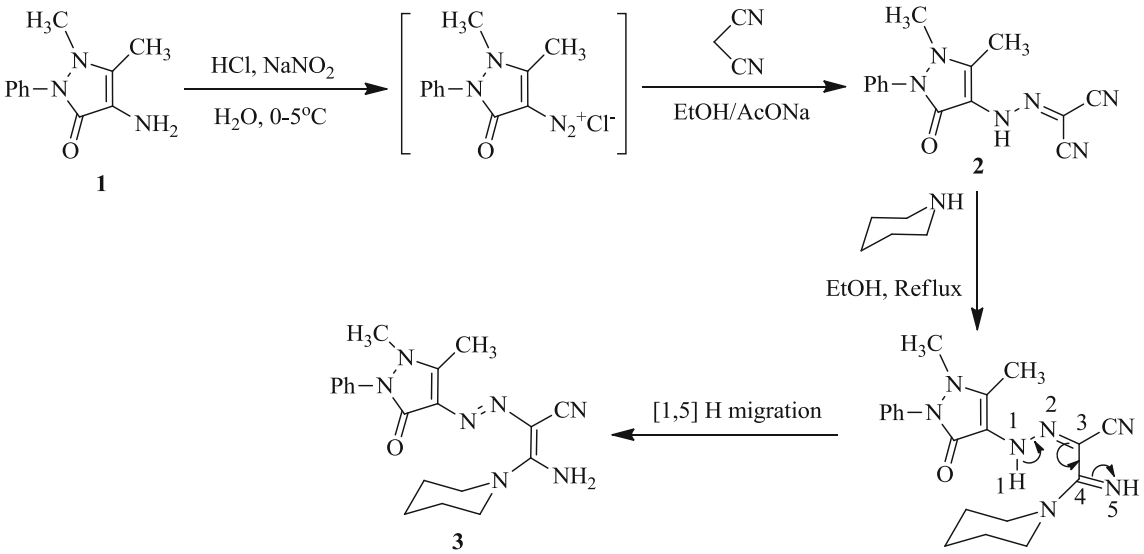

Fig. 1 Synthesis of acyclic enaminonitrile derivative (**3**)

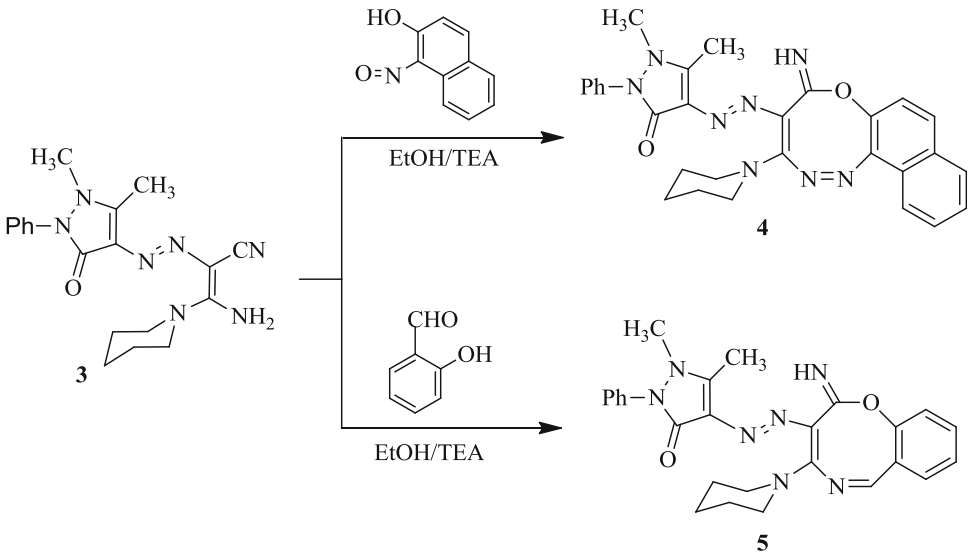

Fig. 2 Synthesis of antipyrinyl derivatives **4** and **5**

acetone, dried at room temperature and kept in a desiccator. After weighing accurately by a digital balance with sensitivity of ±0.1 mg, the specimens were immersed in solution containing 1.0 M HCl solution with and without various concentrations of inhibitors. After 6.0 h exposure, the specimens were taken out rinsed thoroughly with distilled water, dried and weighted accurately again. The average weight loss (W) in g was calculated using the following equation:

$$W = W_1 - W_2 \quad (1)$$

where W_1 and W_2 are the average weight of specimens before and after exposure, respectively. The corrosion rate, v (mm year^{-1}), was calculated using the equation:

$$v = 87{,}600 \times (W/S \times d \times t) \quad (2)$$

where W is the average weight loss (g), S is the surface area of specimens (cm^2), d is the density of iron (7.87 g cm^{-3}) and t is the exposure time (h).

Electrochemical measurements

Electrochemical experiments performed in a conventional three-electrode cell consisting of "a mild steel as working electrode (WE) with exposure surface of 1.0 cm^2, a 1.5 cm × 1.5 cm platinum as counter electrode (CE) and a saturated calomel electrode (SCE) as reference electrode (RE)" were used for measurements. The electrochemical experiments were performed using a Gamry PCI4G750 Potentiostat/Galvanostat/ZRA analyzer, with a Gamry framework system based on ESA400. Gamry applications include dc 105 corrosion software for potentiodynamic polarization measurements, EIS300 software for EIS measurements and Echem Analyst 5.5 software for results plotting, graphing, data fitting and calculating. A computer was used for collecting data.

In the case of potentiodynamic polarization curves, the potential sweep rate was 0.5 mV/s, and the scan potential range was changed automatically from −300 to 300 mV versus open circuit potential (E_{corr}).

The electrochemical impedance spectroscopy (EIS) measurements were carried out at E_{corr}. After the determination of steady-state current at a given potential, sine wave voltages (10 mV), peak to peak, were applied at frequencies between 100 kHz and 10 mHz.

Prior to every experiment, the surface area of mild steel electrode exposed to the solution containing 1.0 M HCl solution with and without various concentrations of inhibitors was abraded, washed by distilled water, degreased with acetone and dried at room temperature as described in weight loss measurements.

Theoretical calculations

Quantum chemical calculations have been widely used to study the reaction mechanisms and to interpret the experimental results as well as to resolve chemical ambiguities. All the calculations were performed using *DMol*^{3} program [22] in Materials Studio package [23], which is designed for the realization of large-scale density functional theory (DFT) calculations. DFT semi-core pseudopods calculations (dspp) were performed with the double numerical basis sets plus polarization functional (DNP). This computational method has been proven to yield satisfactory results. The easiest way to compare the inhibition efficiency of inhibitor is to analyze the energies of the highest occupied molecular orbital (HOMO) and the lowest unoccupied molecular orbital (LUMO). *DMol*^{3} includes certain COSMO[1] [24] controls, which allow for the treatment of solvation effects, so the quantum calculations in aqueous medium were taken.

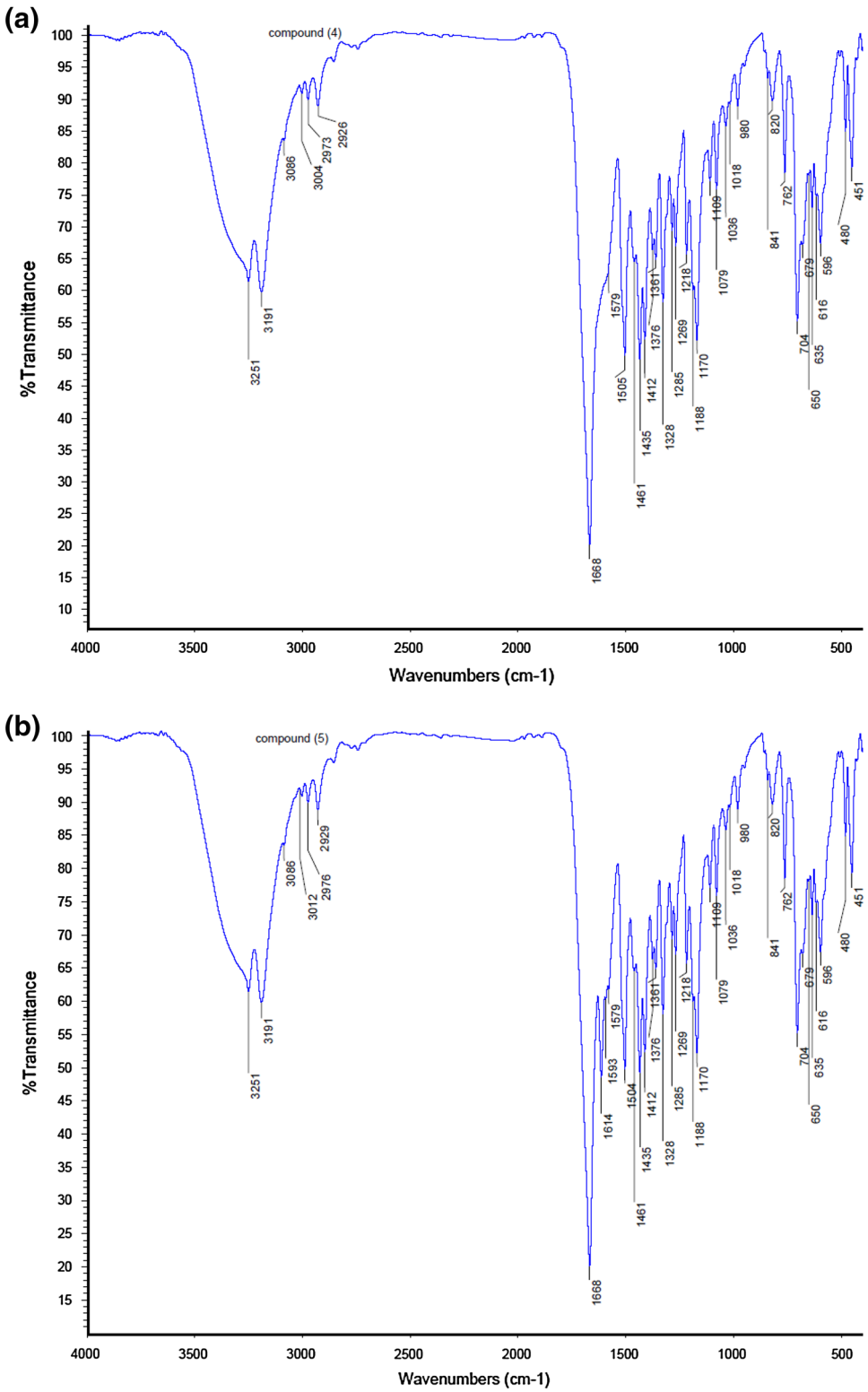

Fig. 3 **a** FTIR spectra of derivative (**4**). **b** FTIR spectra of derivative (**5**)

Results and discussion

Weight loss measurements

Based on weight loss measurements, the weight loss (W), the corrosion rate (v) and the values of inhibition efficiency ($P\%$) for various concentrations of inhibitors after 6.0 h of immersion of mild steel in 1.0 M HCl solution at 298 K are expressed in percentage and given in Table 1.

The inhibition efficiencies ($P\%$) and surface coverages (θ) were calculated using the following equation:

$$P\% = \theta \times 100 = [1 - (v_2/v_1)] \times 100 \quad (3)$$

where v_1 and v_2 are corrosion rates in the absence and presence of inhibitor.

It can be seen from Table 1 that the addition of inhibitor concentrations to the aggressive solution reduces the corrosion rate of mild steel, and hence the inhibition efficiency ($P\%$) increased, suggesting that the inhibitor molecules act by adsorption on the metal surface.

The ranking of the synthesized antipyrinyl derivatives according to their inhibition efficiencies is in the following sequence: (**4**) > (**5**).

In our work, the inhibition efficiency ($P\%$) obtained from weight loss measurements was found to be (87.5 %). Popova et al. [25] found that the ($P\%$) of quaternary ammonium bromides of *N*-containing heterocycles for mild steel corrosion in 1.0 M HCl is (88.8 %), and Solmaza et al. [26] found that the ($P\%$) of 2-((5-mercapto-1,3,4-thiadiazol-2-ylimino) methyl)phenol for mild steel corrosion in 0.5 M HCl is (85.7 %).

Potentiodynamic polarization measurements

The potentiodynamic polarization curves of mild steel in 1.0 M HCl solution in the absence and presence of various concentrations of antipyrinyl derivatives at 25 ± 1 °C are shown in Fig. 4a, b. Our measured free corrosion potential was found to be (−437 mV) for mild steel in 1.0 M HCl. Solmaza et al. [27] found that the free corrosion potential for mild steel in 0.5 M HCl is (−460 mV), Singh et al. [28] found the free corrosion potential for mild steel in 1.0 M HCl is (−472 mV) and Mahdavian and Ashhari [29] found it to be (−479 mV) for mild steel in 1.0 M HCl. From these results, one can conclude that, the free corrosion potential depends on both the composition of the electrode and the concentration of electrolyte used.

Table 1 The data obtained from weight loss measurements for mild steel in 1.0 M HCl solutions in the absence and presence of different concentrations of antipyrinyl derivatives at 25 ± 1 °C

Inhibitor	Conc. (μM)	Wt loss (g)	v (mm year^{-1})	θ	$P\%$
	Blank	2.2	5.17	0.00	00.0
4	2.0	0.458	1.08	0.792	79.2
	4.0	0.387	0.91	0.824	82.4
	6.0	0.328	0.77	0.851	85.1
	8.0	0.282	0.66	0.875	87.5
5	2.0	0.482	1.13	0.781	78.1
	4.0	0.411	0.97	0.813	81.3
	6.0	0.348	0.82	0.842	84.2
	8.0	0.306	0.72	0.861	86.1

The values of related electrochemical parameters, i.e., corrosion potential (E_{corr}), corrosion current density (i_{corr}), cathodic Tafel slope (β_c), anodic Tafel slope (β_a), corrosion rate v (mm year^{-1}) and inhibition efficiency ($P\%$) were calculated from the related polarization curves and are given in Table 2. The inhibition efficiency ($P\%$) and (θ) was calculated from polarization measurements according to the equation given below:

$$P\% = \theta \times 100 = \left[1 - \left(i_{corr}/\, i^*_{corr}\right)\right] \times 100 \quad (4)$$

where i^*_{corr} and i_{corr} are the uninhibited and the inhibited corrosion current densities, respectively.

Corrosion current densities were obtained by the extrapolation of the current–potential lines to the corresponding corrosion potentials. Here in, the corrosion rates were calculated assuming that the whole surface of mild steel is attacked by corrosion and no local corrosion is observed. The corrosion rates v (mm year^{-1}) from polarization were calculated using the following Eq. [30]:

$$v = 10 \times (i_{corr} \times M \times t/F \times S \times d) \quad (5)$$

where M is the molar mass of iron (g mol^{-1}), and F is Faraday constant.

As results obtained from Fig. 3a, b, the addition of inhibitors to the corrosive solution both reduces anodic dissolution of mild steel and also retards cathodic hydrogen evolution reactions as would be expected. The corrosion current density as well as corrosion rate of mild steel is considerably reduced in the presence of the inhibitors. These results are indicative of the adsorption of inhibitors molecules on the mild steel surface.

The inhibition of both anodic and cathodic reactions is more and more pronounced with the increasing inhibitors concentration while the corrosion potential nearly remained the same in comparison with corrosion potential observed in blank solution. These results suggest that inhibitors can be classified as the mixed-type corrosion inhibitors, but it is more polarized to anodic site when an external current was applied [31]. The data in Table 2 indicate that the i_{corr} decreases and the inhibition efficiency ($P\%$) increases as the concentration of the inhibitor increases. In fact the slopes of the cathodic (β_c) and anodic (β_a) Tafel lines (Table 2) are slightly changed upon

Table 2 Electrochemical parameters obtained from potentiodynamic polarization measurements for mild steel in 1.0 M of HCl in the absence and presence of different concentrations of antipyrinyl derivatives at 25 ± 1 °C

Inhibitor	Conc. (μM)	$-E_{corr}$ (mV)	i_{corr} (μA cm^{-2})	$-\beta_c$ (mV dec^{-1})	β_a (mV dec^{-})^{1}	v (mm year^{-1})	θ	$P\%$
	Blank	437	116.2	119	79	128.2	0.000	00.0
4	2.0	405	26.4	97	50.2	29.13	0.773	77.3
	4.0	386	16.4	97	46	18.09	0.859	85.9
	6.0	381	15.0	100	44	16.55	0.871	87.1
	8.0	370	14.4	103	44	15.89	0.876	87.6
5	2.0	438	30.1	115	61	32.3	0.740	74.0
	4.0	424	22.7	101	49	25.04	0.805	80.5
	6.0	417	16.9	104	45	18.65	0.855	85.5
	8.0	391	16.1	103	43	17.76	0.861	86.1

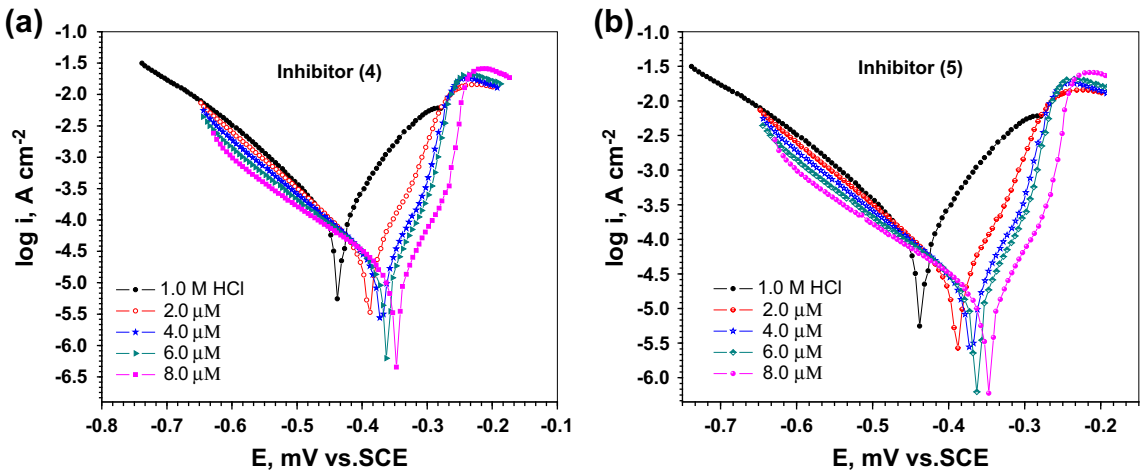

Fig. 4 Potentiodynamic polarization curves for the corrosion of mild steel in 1.0 M HCl in the absence and presence of various concentrations of antipyrinyl derivatives at 25 ± 1 °C

addition of the inhibitors indicating that inhibitors act by simply blocking the available surface area [32].

The ranking of antipyrinyl derivatives remains unchanged; it is as follows: (**4**) > (**5**). This is also in agreement with the observed order of corrosion inhibition obtained from weight loss measurements.

Electrochemical impedance spectroscopy measurements

Impedance spectra for mild steel in 1.0 M HCl in the absence and presence of different concentrations of antipyrinyl derivatives at 25 ± 1 °C are shown in the Nyquist plots (Fig. 5a, b). Clearly, the Nyquist plots indicate that the impedance behavior of mild steel is significantly changed after addition of inhibitor. Nyquist plots consist of a semicircle with one capacitive loop; and the semicircle has a center under the real axis. Such behavior is characteristic for solid electrodes and is often referred to as frequency dispersion. It is attributed to roughness and other in homogeneities of solid surface [33–35]. The diameters of the capacitive loop obtained increase in the presence of inhibitor and are indicative of the degree of inhibition of the corrosion process. The impedance spectra for Nyquist plots were analyzed by fitting to the equivalent circuit model [32, 36], which was used to describe an iron/acid interface given in Fig. 6. The charge transfer resistance (R_{ct}) values are calculated from the difference in impedance at lower and higher frequencies. To obtain the double-layer capacitance (C_{dl}), the frequency at which the imaginary component of the impedance is maximal ($-Z_{max}$) is found using the following equation:

$$C_{dl} = (1/2\pi f_{max} R_{ct}) \quad (6)$$

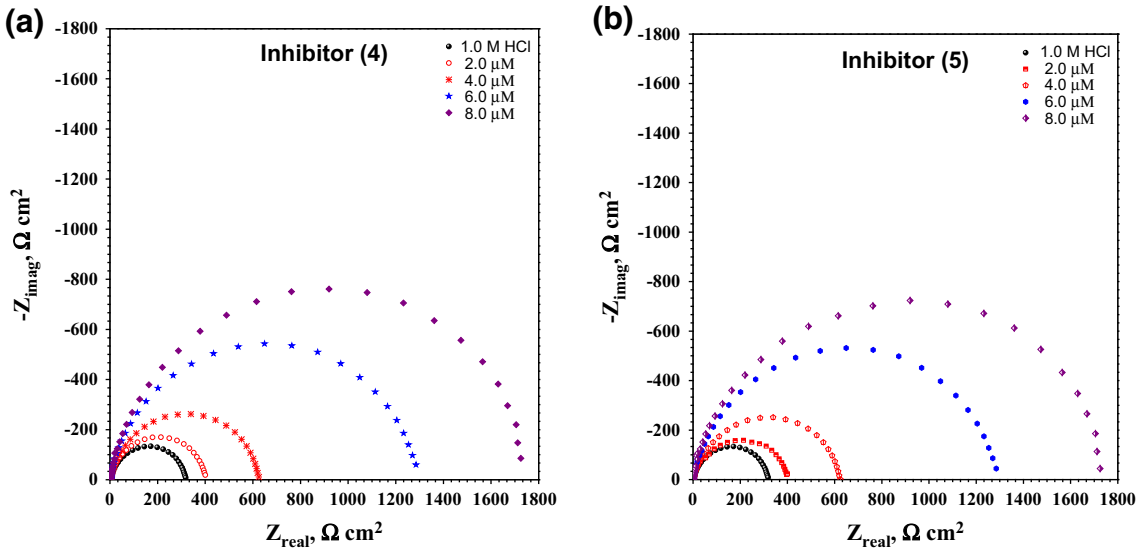

Fig. 5 Nyquist plots for mild steel electrode immersion in 1.0 M HCl solutions without and with various concentrations of antipyrinyl derivatives at 25 ± 1 °C

Table 3 Electrochemical parameters obtained from EIS measurements for mild steel in 1.0 M HCl in the absence and presence of different concentrations of antipyrinyl derivatives at 25 ± 1 °C

Inhibitor	Conc. (µM)	R_s (Ω cm^2)	C_{dl} (µF cm^{-2})	R_{ct} (Ω cm^2)	θ	$P\%$
	Blank	3.2	27.3	315.0	0.000	00.0
4	2.0	2.9	16.6	417.0	0.245	24.5
	4.0	3.6	8.45	624.0	0.495	49.5
	6.0	2.8	2.43	1291.0	0.760	76.0
	8.0	2.4	1.18	1729.0	0.820	82.0
5	2.0	2.8	15.9	405.0	0.220	22.0
	4.0	2.4	9.15	619.0	0.491	49.1
	6.0	3.4	3.75	1276.0	0.753	75.3
	8.0	2.7	2.94	1720.0	0.817	81.7

where f_{max} is the frequency at the maximum in the Nyquist plot, R_{ct} is the charge transfer resistance value, and C_{dl} is the double-layer capacitance.

The inhibition efficiency ($P\%$) and (θ) obtained from the charge transfer resistance was calculated by the following equation:

$$P\% = \theta \times 100 = \left[1 - \left(R_{ct}/R^*_{ct}\right)\right] \times 100 \quad (7)$$

where R^*_{ct} and R_{ct} are the charge transfer resistance values with and without inhibitor, respectively. The data are collected in Table 3. The results demonstrated that the charge transfer (R_{ct}) values increased and the double-layer capacitance (C_{dl}) values decreased with an increase in inhibitor concentration. The increase in the (R_{ct}) values with inhibitor concentration indicates an increase in the surface coverage by the inhibitor molecules, resulting in an increase in inhibitor efficiency [37]. The decrease in (C_{dl}) values, which can result from a decrease in the local dielectric constant and/or an increase in the thickness of the electrical double layer, suggests that the inhibitors act by adsorption at the metal solution/interface [38]. The EIS results confirm the results obtained from weight loss and potentiodynamic polarization measurements that the inhibition efficiency ($P\%$) of the synthesized antipyrinyl derivatives is in the same sequence as follows: (**4**) > (**5**).

Effect of temperature and activation energy

The effect of temperature on the inhibited acid–metal reaction is highly complex because many changes occur on the metal surface such as rapid etching and inhibitor, desorption and decomposition and/or rearrangement [39]. To evaluate the adsorption of inhibitors and activation parameters of the corrosion processes of mild steel surface in acidic media, the weight loss parameters were investigated in the absence and presence of inhibitors at temperature range of 298–328 K. The relationship between the

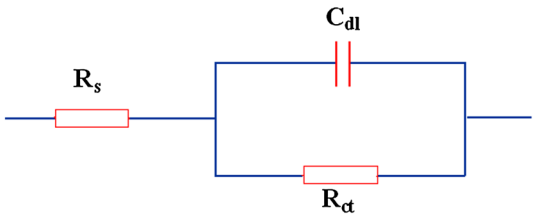

Fig. 6 Equivalent circuit model used to fit the impedance spectra (R_s = solution resistance, R_{ct} = charge transfer resistance, and C_{dl} = double-layer capacitance)

corrosion rate of mild steel in acidic media and temperature is often expressed by the Arrhenius equation:

$$v_{corr} = A \exp\left(-E_a^*/RT\right) \quad (8)$$

where v_{corr} is corrosion rate, A is the constant, E_a^* is the activation energy of the metal dissolution reaction, R is the gas constant and T is the absolute temperature. The E_a^* values can be determined from the slop of Arrhenius plots (log v_{corr} versus $1/T$) as shown in Fig. 7. Calculated E_a^* values, corrosion rate and inhibition efficiencies are listed in Table 4. As seen in Table 4, E_a^* in the inhibited solution is higher than that obtained for the free acid solution indicating that the corrosion reaction of mild steel is inhibited by inhibitors and hence supports the phenomenon of physical adsorption [40, 41]. Higher values of E_a^* in the presence of inhibitor can be correlated with increasing thickness of the double layer which enhances the E_a^* of the corrosion process [42]. It is also an indication of a strong inhibitive action of inhibitors by increasing energy barrier for the corrosion process, emphasizing the electrostatic character of the inhibitor's adsorption on the mild steel surface (physisorption) [43].

Adsorption isotherm and thermodynamic parameters

The action of an inhibitor in aggressive acid media is assumed to be due to its adsorption at the metal/solution interface. The adsorption process depends on the electronic characteristics of the inhibitor, the nature of metal surface, temperature, steric effects and the varying degrees of surface-site activity [44]. In fact, the solvent H_2O molecules could also be adsorbed at the metal/solution interface. Therefore, the adsorption of organic inhibitor molecules from the aqueous solution can be considered as a quasi-substitution process between the organic compounds in the aqueous phase $Org_{(sol)}$ and water molecules at the electrode surface $H_2O_{(ads)}$ [45]:

$$Org_{(sol)} + x\, H_2O_{(ads)} \leftrightarrow Org_{(adsl)} + x\, H_2O_{(sol)} \quad (9)$$

where x is the size ratio, that is, the number of water molecules replaced by one organic inhibitor. The type of the adsorption isotherm can provide additional information about the properties of the tested compounds. To obtain the adsorption isotherm, the degree of surface coverage [$\theta = (P/100)$] of the inhibitor must be calculated. In this study, the degree of surface coverage values (θ) for various concentrations of the inhibitors in acidic media has been evaluated from the potentiodynamic polarization measurements. Attempts were made to fit the (θ) values to various isotherms, including Langmuir, Temkin, Frumkin and Flory–Huggins. By far, the best fit is obtained with the Langmuir isotherm. Langmuir adsorption isotherm is described by the following equations:

$$C_{inh}/\theta = 1/K_{ads} + C_{inh} \quad (10)$$

where C_{inh} is the inhibitor concentration, K_{ads} is the adsorption equilibrium constant and θ is the surface coverage. Figure 8 shows the plots of C_{inh}/θ versus C_{inh} and the expected linear relationship is obtained for inhibitors. The strong correlations ($R^2 = 0.999$) confirm the validity of this approach. The slop of the straight lines equal the unity, suggesting that the adsorbed inhibitor molecules form monolayer on the mild steel surface and there is no interaction among the adsorbed inhibitor molecules [46]. On the other hand, the intercept of straight lines equal to the reciprocal of equilibrium constant ($1/K_{ads}$), the relatively high values of $1/K_{ads}$ (Table 5), reflects the high adsorption ability of inhibitors on mild steel surface [47, 48]. The standard free energy of adsorption (ΔG_{ads}^o) can be given as the following equation:

$$K_{ads} = (1/55.5) \exp\left(-\Delta G_{ads}^o/RT\right) \quad (11)$$

where the value 55.5 is the concentration of water in solution expressed in Molar [49]. The ΔG_{ads}^o values are calculated and listed in Table 5.

The negative values of ΔG_{ads}^o indicated that the adsorption of inhibitor molecule is a spontaneous process. Generally, it is well known that values of ΔG_{ads}^o are of the order of -20 kJ mol^{-1} or lower indicating the electrostatic interaction between the charged molecules and the charged metal (physical adsorption); those of order of -40 kJ mol^{-1} or higher involve sharing or transfer of electrons from the inhibitor molecules to the metal surface to form a co-ordinate type of bond (chemisorption) [50]. In our experiment, the value of ΔG_{ads}^o is -46.7 kJ mol^{-1}, indicating that the adsorption mechanism of the inhibitors on mild steel in 1.0 M HCl solution is neither typical physisorption nor typical chemisorption but it is complex mixed type and electrostatic interaction (physisorption) is predominant [51–53].

Another form of Langmuir equation is written as below:

$$\theta/1 - \theta = AC \exp\left(-\Delta H_{ads}^o/RT\right) \quad (12)$$

Table 4 Corrosion rate, inhibition efficiency and activation energy values of the dissolution of mild steel in 1.0 M HCl in the absence and presence of 8.0 μM of antipyrinyl derivatives at different temperatures

T (K)	Blank		Inhibitor (**4**)			Inhibitor (**5**)		
	v (mm year^{-1})	E_a^* (kJ/mol)	v (mm year^{-1})	E_a^* (kJ/mol)	P%	v (mm year^{-1})	E_a^* (kJ/mol)	P%
298	5.17	22.8	0.66	27.1	87.5	0.72	28.0	86.1
308	6.31		0.96		84.7	1.06		83.2
318	7.47		1.32		82.3	1.41		81.1
328	8.95		1.78		80.1	2.05		77.1

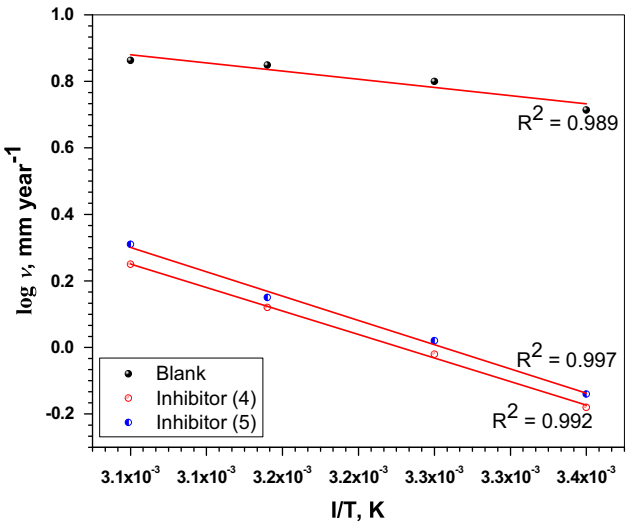

Fig. 7 Log corrosion rate (mm year^{-1}) versus 1/T curves for mild steel dissolution in 1.0 M HCl in the absence and presence of 8.0 μM of antipyrinyl derivatives

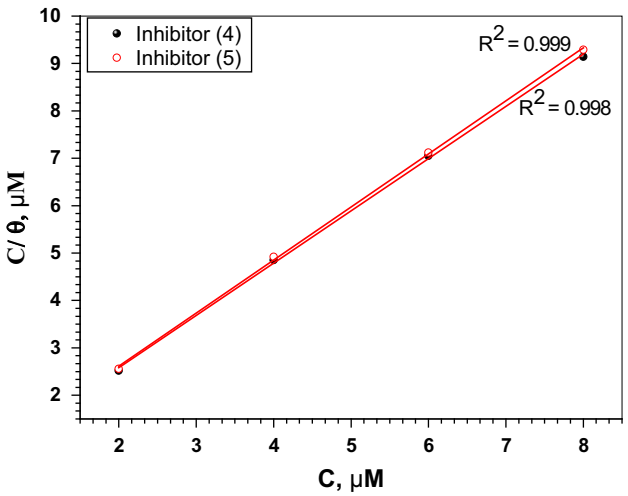

Fig. 8 Adsorption isotherm curves for the adsorption of antipyrinyl derivatives on mild steel in 1.0 M HCl at 25 ± 1 °C

Table 5 Thermodynamic parameters for the adsorption of antipyrinyl derivatives on the mild steel in 1.0 M HCl

Inhibitor	K_{ads} (M^{-1})	$-\Delta G^o_{ads}$ (kJ mol^{-1})	$-\Delta H^o_{ads}$ (kJ mol^{-1})	$-\Delta S^o_{ads}$ (J mol^{-1} K^{-1})
4	2.67 × 10^6	46.7	54.0	24.5
5	2.65 × 10^6	46.6	54.2	25.5

where A is the independent constant, C is the inhibitor concentration, ΔH^o_{ads} is the standard heat of adsorption, and θ is the surface coverage by the inhibitor molecules. The log [$\theta/(1-\theta)$] versus 1/T at the optimum concentration of inhibitors is plotted (Fig. 9). The slopes of the linear part of the plot are equal to $-\Delta H^o_{ads}/R$, from which the heat of adsorption (ΔH^o_{ads}) values was calculated and listed in Table 5. The negative value of (ΔH^o_{ads}) indicates that the adsorption of inhibitors is an exothermic process, which suggests that inhibition efficiency decreases with the increase in temperature [54]. Such behavior can also be interpreted on the basis that the increase in temperature resulted in desorption of some adsorbed inhibitor molecules from the steel surface. Standard adsorption entropy (ΔS^o_{ads}) is calculated from the below equation:

$$\Delta G^o_{ads} = \Delta H^o_{ads} - T\Delta S^o_{ads} \quad (13)$$

From the Eq. (13), the value of ΔS^o_{ads} was calculated and listed in Table 5. The value of ΔS^o_{ads} is negative, which implies that a decrease in disordering takes place on going from reactants to the metal adsorbed species reaction complex [55].

Prediction of theoretical parameters

According to the DFT, the reactive ability of the inhibitor is related with the frontier molecular orbitals (MO) that are the HOMO and the LUMO [56]. Higher HOMO energy (E_{HOMO}) of the adsorbent leads to higher electron donating ability [57]. Low LUMO energy (E_{LUMO}) indicates that the acceptor accepts electrons easily.

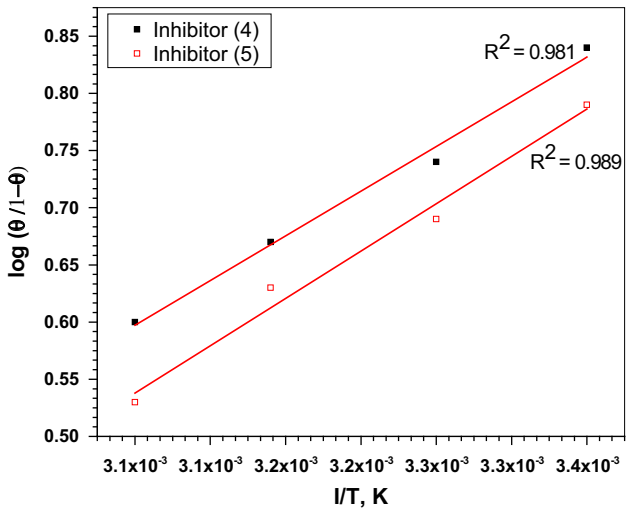

Fig. 9 Log $[\theta/(1-\theta)]$ versus $1/T$ at the optimum concentration (8.0 μM) of inhibitors for corrosion of mild steel in 1.0 M HCl solution

Table 6 Theoretical parameters calculated at DFT level for antipyrinyl derivatives

Inhibitor	E_{HOMO} (eV)	E_{LUMO} (eV)	ΔE_{L-H} (eV)	μ (D)	$P\%$
4	−1.167	−0.115	1.052	4.768	87.5
5	−1.282	−0.119	1.163	4.124	86.1

The energy of the highest occupied molecular orbital (E_{HOMO}), energy of the lowest unoccupied molecular orbital (E_{LUMO}) and energy gap (ΔE_{L-H}) between LUMO and HOMO were determined by optimization. The optimized molecular structures, the HOMO and LUMO electronic density distributions of these inhibitors are shown in Fig. 10. For the HOMO of the studied compounds, it can be observed that the benzene rings, –C, N– and O–, have a large electron density.

The calculated quantum chemical parameters are given in Table 6. The HOMO and LUMO energies are correlated with percent inhibition efficiencies ($P\%$). The percent inhibition efficiencies ($P\%$) increase if the molecules have higher HOMO energies and lower LUMO energies [58]. The percent inhibition efficiency ($P\%$) increased with decrease in energy gap (ΔE_{L-H}). The values for E_{HOMO}, E_{LUMO} and ΔE_{L-H} (Table 6) show that inhibitor (**4**) has a somewhat more ability to act as corrosion inhibitor than inhibitor (**5**). The data presented in Table 6 show that the calculated dipole moment (μ) for inhibitor (**4**) has the highest dipolar moment than (**5**) and, consequently, the reactivity of the molecule on the surface is hugely facilitated [59].

Mechanism of inhibition

The first stage in the mechanism of inhibition in acid media is adsorption on the metal surface [60]. In most inhibition

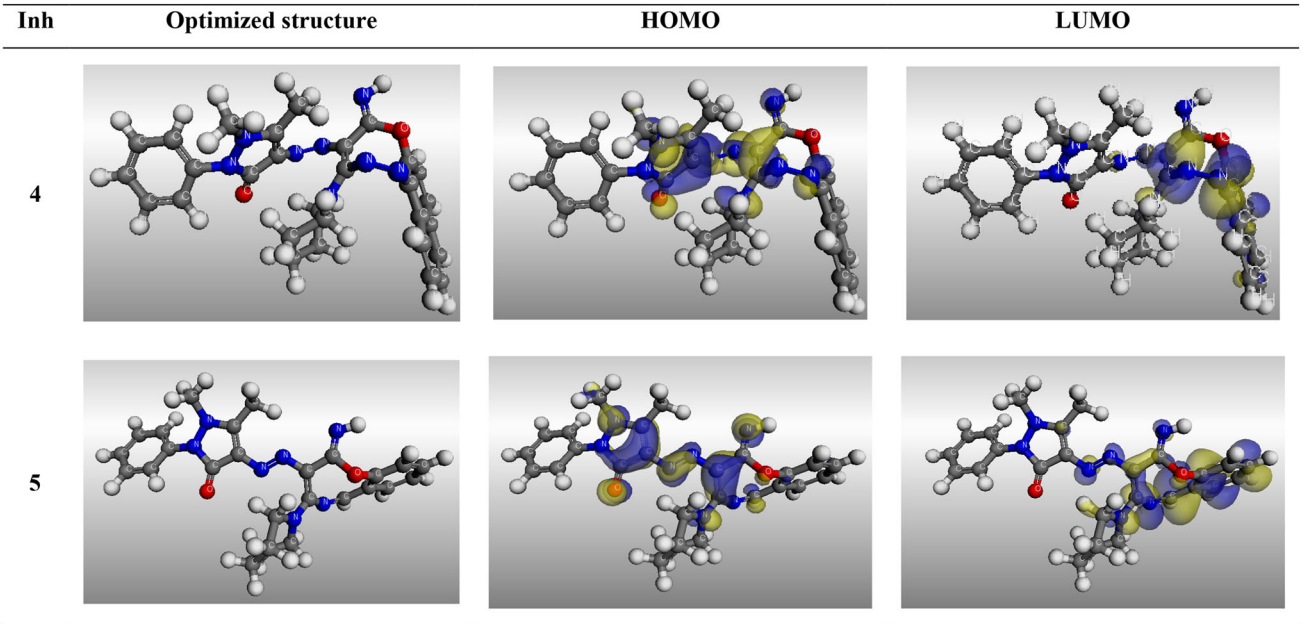

Fig. 10 Optimized molecular structures, highest occupied molecular orbital (HOMO) and lowest occupied molecular orbital (LUMO) for antipyrinyl derivatives

studies, the formation of a donor acceptor surface complex between π-electrons of the inhibitor and the vacant *d*-orbitals of the metal is postulated [61–63]. Inhibitor has many N-, O-atoms and aromatic rings. In aqueous acidic solutions, the inhibitor is either neutral or in the form of cations (i.e., protonated species). In general, two modes of adsorption may be considered. The neutral form of the inhibitor may adsorb on the metal surface via the chemisorption mechanism involving the displacement of water molecules from the metal surface and the sharing electrons between N- and O-atoms and Fe and/or between π-electrons of the aromatic ring and the vacant *d*-orbitals of Fe. On the other hand, it is well known that the mild steel surface is positively charged in the acidic media [64]. Therefore, it is difficult for a protonated inhibitor to adsorb on the positively charged steel surface due to electrostatic repulsion. Since chloride ions (Cl^-) have a smaller degree of hydration, being specifically adsorbed, they create an excess negative charge toward the solution and favor more adsorption of the protonated inhibitor. In other words, there may be a synergism between Cl^- and the inhibitor, which improves the inhibitive capability of the inhibitor. When the protonated inhibitor is adsorbed on the metal surface, the following may be happened: (1) formation of a coordinate bond due to the partial transfer of electron from N- and O-atoms to the metal surface and (2) the protonated inhibitor may combine with freshly generated Fe^{2+} ions on the mild steel surface to form a metal-inhibitor complex $[Inh_z–Fe]^{(2+z)+}$ [65]. This complex may become adsorbed onto the steel surface by Van der Waals forces to form a protective film, thereby preventing corrosion. The film covers both the anodic and cathodic reactive sites on the steel surface, and inhibits both reactions at the same time.

The difference in the inhibition efficiencies (*P*%) between inhibitor (**4**) and (**5**) can be explained on the basis of heteroatoms with high electron density (O and N) which are considered as adsorption active sites, in addition to π-electrons of the aromatic ring. It is clear that inhibitor (**4**) exhibits excellent (*P*%) due to bearing (2O, 8 N and two aromatic benzene rings), so it is more adsorbed on the surface of metal giving more inhibition efficiency. On the contrary, inhibitor (**5**) comes after inhibitor (**4**) in (*P*%) because it has (2O, 7 N and one aromatic benzene ring) only.

Conclusions

The corrosion rates and inhibition efficiencies of mild steel were monitored and controlled in 1.0 M HCl solutions at different temperatures without and with various concentrations of new synthesized antipyrinyl derivatives. Chemical (weight loss) and electrochemical (potentiodynamic polarization and impedance) methods were employed in the present work. The principle conclusions are: (1) The inhibition efficiency increases with the increase in inhibitor concentration, while it decreases with temperature, suggesting the occurrence of physical adsorption. (2) Potentiodynamic polarization plots indicated that the tested synthesized antipyrinyl derivatives act as mixed-type inhibitors. (3) Langmuir adsorption isotherm exhibited the best fit to the experimental data with $-\Delta G^o_{ads}$ of 46.7 and 46.6 kJ mol^{-1} for compounds 4 and 5, respectively, which indicate that the adsorption mechanism of the inhibitors on mild steel in 1.0 M HCl solution is neither typical physisorption nor typical chemisorption but it is complex mixed type and electrostatic interaction (physisorption) is predominant. (4) The high value of K_{ads} suggested that antipyrinyl derivatives molecules strongly adsorb on the mild steel surface. (5) Apparent activation energies (E^*_a) in the presence of these inhibitors are higher than those in HCl solution. (6) Through DFT quantum chemical calculations, a correlation between parameters related to the electronic structure of antipyrinyl derivatives and their ability to inhibit the corrosion process could be established. The calculated energy gaps show reasonably good correlation with the efficiency of corrosion inhibition.

References

1. Ahamad I, Quraishi MA (2009) Bis(benzimidazol-2-yl) disulphide: an efficient water soluble inhibitor for corrosion of mild steel in acid media. Corros Sci 51:2006–2013
2. Zhang QB, Hua YX (2009) Corrosion inhibition of mild steel by alkylimidazolium ionic liquids in hydrochloric acid. Electrochim Acta 54:1881–1887
3. Li W, He Q, Pei C, Hou B (2007) Experimental and theoretical investigation of the adsorption behaviour of new triazole derivatives as inhibitors for mild steel corrosion in acid media. Electrochim Acta 52:6386–6394
4. Solmaz R, Kardas G, Yazıcı B, Erbil M (2005) Inhibition effect of rhodanine for corrosion of mild steel in hydrochloric acid solution. Prot Met 41:581–585
5. Kardas G (2005) The inhibition effect of 2-thiobarbituric acid on the corrosion performance of mild steel in HCl solutions. Mater Sci 41:337–343
6. Khamis A, Saleh MM, Awad MI, El-Anadouli BE (2013) Enhancing the inhibition action of cationic surfactant with sodium halides for mild steel in 0.5 M H_2SO_4. Corros Sci 74:168–177
7. El-Haddad MN, Fouda AS (2013) Inhibition effect and adsorption behavior of new azodye derivatives on corrosion of carbon steel in acid medium. J Disper Sci Technol 34:1471–1480
8. El-Haddad MN, Fouda AS (2013) Corrosion inhibition and adsorption behavior of some azo dye derivatives on carbon steel in

acidic medium: synergistic effect of halide ions. Chem Eng Commun 200:1366–1393
9. Abd El Maksoud SS (2002) Studies on the effect of pyranocoumarin derivatives on the corrosion of iron in 0. 5 M HCl. Corros Sci 44:803–813
10. Abdallah M (2002) Rhodanine azosulpha drugs as corrosion inhibitors for corrosion of 304 stainless steel in hydrochloric acid solution. Corros Sci 44:717–728
11. Hu J, Zeng D, Zhang Z, Shi T, Song G, Guo X (2013) 2-Hydroxy-4-methoxy-acetophenone as an environment-friendly corrosion inhibitor for AZ91D magnesium alloy. Corros Sci 74:35–43
12. Ghailane T, Balkhmima RA, Ghailane R, Souizi A, Touir R, Ebn Touhami M, Marakchi K, Komiha N (2013) Experimental and theoretical studies for mild steel corrosion inhibition in 1 M HCl by two new benzothiazine derivatives. Corros Sci 76:317–324
13. Moretti G, Guidi F, Fabris F (2013) Corrosion inhibition of the mild steel in 0.5 M HCl by 2-butyl-hexahydropyrrolo[1,2-b][1,2]oxazole. Corros Sci 76:206–218
14. Pournazari SH, Moayed MH, Rahimizadeh M (2013) In situ inhibitor synthesis from admixture of benzaldehyde and benzene-1,2-diamine along with $FeCl_3$ catalyst as a new corrosion inhibitor for mild steel in 0.5 M sulphuric acid. Corros Sci 71:20–31
15. Yadav DK, Quraishi MA, Maiti B (2013) Inhibition effect of some benzylidenes on mild steel in 1 M HCl: an experimental and theoretical correlation. Corros Sci 55:254–266
16. El-Haddad MN, Elattar KM (2012) Role of novel oxazocine derivative as corrosion inhibitor for 304 stainless steel in acidic chloride pickling solutions. Res Chem Intermed 39:3135–3149
17. Liu B, Liu Z, Han G, Li Y (2011) Corrosion inhibition and adsorption behavior of 2-((dehydroabietylamine)methyl)-6-methoxyphenol on mild steel surface in seawater. Thin Solid Films 519:7836–7844
18. Obot IB, Ebenso EE, Kabanda MM (2013) Metronidazole as environmentally safe corrosion inhibitor for mild steel in 0.5 M HCl: experimental and theoretical investigation. J Environ Chem Eng 1:431–439
19. Zhang S, Tao Z, Li W, Hou B (2009) The effect of some triazole derivatives as inhibitors for the corrosion of mild steel in 1 M hydrochloric acid. Appl Surf Sci 255:6757–6763
20. Kryštof V, Cankař P, Fryšová I, Slouka J, Kontopidis G, Džubák P, Hajdúch M, Srovnal J, de Azevedo WF Jr, Orság M, Paprskářová M, Rolčík J, Látr A, Fischer PM, Strnad M (2006) 4-Arylazo-3,5-diamino-1*H*-pyrazole CDK inhibitors: SAR study, crystal structure in complex with CDK2, selectivity, and cellular effects. J Med Chem 49:6500–6509
21. Fadda AA, Etman HA, El-Seidy MY, Elattar KM (2012) Utility of enaminonitriles in heterocyclic synthesis: synthesis of some new pyrazole, pyridine, and pyrimidine derivatives. J Heterocycl Chem 49:774–781
22. Wu X, Ray AK (2002) Density-functional study of water adsorption on the PuO_2(110) surface. Phys Rev B 65:85403–85409
23. Materials studio v 5.0, copyright Accelrys software Inc (2009)
24. Mulliken RS (1955) Electronic population analysis on LCAO–MO molecular wave functions. J Chem Phys 23:1833–1840
25. Popova A, Christov M, Vasilev A (2007) Inhibitive properties of quaternary ammonium bromides of N-containing heterocycles on acid mild steel corrosion. Part I: gravimetric and voltammetric results. Corros Sci 49:3276–3289
26. Solmaza R, Altunbas E, Kardas G (2011) Adsorption and corrosion inhibition effect of 2-((5-mercapto-1,3, 4-thiadiazol-2-ylimino)methyl)phenol Schiff base on mild steel. Mater Chem Phys 125:796–801
27. Solmaza R, Kardas G, Culha M, Yazici B, Erbil M (2008) Investigation of adsorption and inhibitive effect of 2-mercaptothiazoline on corrosion of mild steel in hydrochloric acid media. Electrochim Acta 53:5941–5952
28. Singh A, Avyaya JN, Ebenso EE, Quraishi MA (2013) Schiff's base derived from the pharmaceutical drug Dapsone (DS) as a new and effective corrosion inhibitor for mild steel in hydrochloric acid. Res Chem Intermed 39:537–551
29. Mahdavian M, Ashhari S (2010) Corrosion inhibition performance of 2-mercaptobenzimidazole and 2-mercaptobenzoxazole compounds for protection of mild steel in hydrochloric acid solution. Electrochim Acta 55:1720–1724
30. Doner A, Solmaz R, Ozcan M, Kardas G (2011) Experimental and theoretical studies of thiazoles as corrosion inhibitors for mild steel in sulphuric acid solution. Corros Sci 53:2902–2913
31. Behpour M, Ghoreishi SM, Soltani N, Salavati-Niasari M (2009) The inhibitive effect of some bis-N, S-bidentate Schiff bases on corrosion behaviour of 304 stainless steel in hydrochloric acid solution. Corros Sci 51:1073–1082
32. Etaiw SEH, Fouda AS, Amer SA, El-bendary MM (2011) Structure, characterization and anti-corrosion activity of the new metal–organic framework [Ag(qox)(4-ab)]. J Inorg Organomet Polym 21:327–335
33. Elayyachy M, El-Idrissi A, Hommouti B (2006) New thio-compounds as corrosion inhibitor for steel in 1 M HCl. Corros Sci 48:2470–2479
34. Hosseini M, Mertens SFL, Ghorbani M, Arshadi MR (2003) Asymmetrical Schiff bases as inhibitors of mild steel corrosion in sulphuric acid media. Mater Chem Phys 78:800–808
35. Martinez S, Metikos-Hukovic M (2003) A nonlinear kinetic model introduced for the corrosion inhibitive properties of some organic inhibitors. J Appl Electrochem 33:1137–1142
36. Mansfeld F (1981) Recording and analysis of AC impedance data for corrosion studies. Corrosion 36:301–307
37. Lebrini M, Lagrenee M, Vezin H, Gengembre L, Bentiss F (2005) Electrochemical and quantum chemical studies of new thiadiazole derivatives adsorption on mild steel in normal hydrochloric acid medium. Corros Sci 47:485–505
38. MCafferty E, Hackerman N (1972) Double layer capacitance of iron and corrosion inhibition with polymethylene diamines. J Electrochem Soc 119:146–154
39. Fekry AM, Mohamed RR (2010) Acetyl thiourea chitosan as an eco friendly inhibitor for mild steel in sulphuric acid medium. Electrochim Acta 55:1933–1939
40. Umoren SA, Obot IB (2008) Polyvinylpyrollidone and polyacrylamide as corrosion inhibitors for mild steel in acidic medium. Surf Rev Lett 15:277–286
41. Kosari A, Momeni M, Parvizi R, Zakeri M, Moayed MH, Davoodi A, Eshghi H (2011) Theoretical and electrochemical assessment of inhibitive behavior of some thiophenol derivatives on mild steel in HCl. Corros Sci 53:3058–3067
42. Singh MR, Bhrara K, Singh G (2008) The inhibitory effect of diethanolamine on corrosion of mild steel in 0.5 M sulphuric acidic medium. Port Electrochim Acta 26:479–492
43. Obot IB, Obi-Egbedi NO (2008) Inhibitory effect and adsorption characteristics of 2,3-diaminonaphthalene at aluminum/hydrochloric acid interface: experimental and theoretical study. Surf Rev Lett 15:903–910
44. Bockris JO'M, Reddy AKN (1976) Modern electrochemistry. Plenum Publishing Corporation, New York
45. Wang X, Yang H, Wang F (2010) A cationic gemini-surfactant as effective inhibitor for mild steel in HCl solutions. Corros Sci 52:1268–1276
46. Ebenso EE, Obot IB, Murulana LC (2010) Quinoline and its derivatives as effective corrosion inhibitors for mild steel in acidic medium. Int J Electrochem Sci 5:1574–1586
47. Migahed MA (2005) Electrochemical investigation of the corrosion behaviour of mild steel in 2 M HCl solution in presence of 1-dodecyl-4-methoxy pyridinium bromide. Mater Chem Phys 93:48–53

48. Wang X, Yang H, Wang F (2011) An investigation of benzimidazole derivative as corrosion inhibitor for mild steel in different concentration HCl solutions. Corros Sci 53:113–121
49. Sudheer M, Quraishi MA (2013) Electrochemical and theoretical investigation of triazole derivatives on corrosion inhibition behavior of copper in hydrochloric acid medium. Corros Sci 70:161–169
50. Yadav M, Behera D, Kumar S, Yadav P (2015) Experimental and quantum chemical studies on corrosion inhibition performance of thiazolidinedione derivatives for mild steel in hydrochloric acid solution. Chem Eng Commun 202:303–315
51. Ghareba S, Omanovic S (2010) Interaction of 12 aminododecanoic acid with a carbon steel surface: towards the development of 'green' corrosion inhibitors. Corros Sci 52:2104–2113
52. Mert BD, Mert ME, Kardas G, Yazıcı B (2011) Experimental and theoretical investigation of 3-amino-1,2,4-triazole-5-thiol as a corrosion inhibitor for carbon steel in HCl medium. Corros Sci 53:4265–4272
53. Pavithra MK, Venkatesha TV, Kumar MKP, Tondan HC (2012) Inhibition of mild steel corrosion by Rabeprazole sulfide. Corros Sci 60:104–111
54. Yuce AO, Kardas G (2012) Adsorption and inhibition effect of 2-thiohydantoin on mild steel corrosion in 0.1 M HCl. Corros Sci 58:86–94
55. Li XH, Deng SD, Fu H (2010) Adsorption and inhibition effect of vanillin on cold rolled steel in 3.0 M H_3PO_4. Prog Org Coat 67:420–426
56. Eddy NO, Ebenso EE (2009) Quantum chemical studies on the inhibition potentials of some penicillin compounds for the corrosion of mild steel in 0.1 M HCl. J Mol Model 16:1291–1306
57. Lee C, Yang W, Parr RG (1988) Development of the Colle–Salvetti correlation-energy formula into a functional of the electron density. Phys Rev B 37:785–789
58. Sastri VS, Perumareddi JR (1997) Molecular orbital theoretical studies of some organic corrosion inhibitors. Corrosion 53:617–622
59. Mihit M, Laarej K, Abou El Makarim H, Bazzi L, Salghi R, Hammouti B (2010) Study of the inhibition of the corrosion of copper and zinc in HNO_3 solution by electrochemical technique and quantum chemical calculations. Arab J Chem 3:55–60
60. Yurt A, Balaban Kaandemir, Bereket G, Erk B (2004) Investigation on some Schiff bases as HCl corrosion inhibitors forcarbon steel. Mater Chem Phys 85:420–426
61. Gomma GK, Wahdan MH (1994) Effect of temperature on the acidic dissolution of copper in the presence of amino acids. Mater Chem Phys 39:142–148
62. Quraishi MA, Sardar R (2003) Corrosion inhibition by fatty acid tria-zoles for mild steel in formic acid. J Appl Electrochem 33:1163–1168
63. Muralidharan S, Quraishi MA, Iyer SKV (1995) The effect of molecular structure on hydrogen permeation and the corrosion inhibition of mild steel in acidic solutions. Corros Sci 37:1739–1750
64. Bentiss F, Traisnel M, Lagrenee M (2000) The inhibition action of 3,6-bis(2-methoxyphenyl)-1,2-dihydro-1,2,4,5-tetrazine on thecorrosion of mild steel in acidic media. Corros Sci 42:127–146
65. Li XH, Deng SD, Fu H (2010) Inhibition by Jasminum nudiflorum Lindl. leaves extract of the corrosion of cold rolled steel in hydrochloric acid solution. J Appl Electrochem 40:1641–1649